ATMOSPHERIC ENVIRONMENT: X 9 (2021) 100104

Contents lists available at ScienceDirect

Atmospheric Environment: X

journal homepage: http://www.journals.elsevier.com/atmospheric-environment-x

Reductions in nitrogen oxides over the Netherlands between 2005 and 2018 observed from space and on the ground: Decreasing emissions and increasing O_3 indicate changing NO_x chemistry

Marina Zara [a,b], K. Folkert Boersma [a,b,*], Henk Eskes [a], Hugo Denier van der Gon [c], Jordi Vilà-Guerau de Arellano [b], Maarten Krol [b,e], Eric van der Swaluw [d], William Schuch [d], Guus J.M. Velders [d,e]

[a] Royal Netherlands Meteorological Institute, De Bilt, the Netherlands
[b] Wageningen University, Environmental Sciences Group, Wageningen, the Netherlands
[c] TNO - The Netherlands Organisation for Applied Scientific Research, Utrecht, the Netherlands
[d] National Institute for Public Health and the Environment, Centre for Environmental Monitoring, P.O. Box 1, 3720, BA Bilthoven, the Netherlands
[e] Institute for Marine and Atmospheric Research Utrecht, Utrecht University, P.O. Box 80011, 3508, TA Utrecht, the Netherlands

ARTICLE INFO

Keywords:
Nitrogen oxides
OMI
Ozone
Trends
Air pollution

ABSTRACT

Satellite measurements of tropospheric NO_2 columns are valuable for monitoring long-term changes in air quality. However, direct linkage of satellite-derived NO_2 trends with changes in underlying NO_x emissions and NO_x surface concentrations is complicated by the contribution of background NO_2 to the column, by changes in the chemical regime wherein emissions take place, and by data sampling differences. Here we study the 2005–2018 changes in nitrogen oxides concentrations over the polluted Netherlands. We use the QA4ECV OMI NO_2 retrievals, RIVM surface measurements of NO, NO_2, and O_3, wet deposition fluxes of nitrate, and NO_x emissions reported in two European inventories (EMEP and TNO-MACC-III). We interpret the observed changes in concentrations with simulations by CLASS, a box model accounting for boundary layer dynamics and chemistry. Nationally averaged, OMI column NO_2 and RIVM surface NO_2 concentrations are reduced by 30% and 32% respectively between 2005 and 2018. This is in line with Dutch national NO_x emissions from the TNO-MACC-III and EMEP inventories showing decreases of 32%–39%, respectively, between 2005 and 2018. There is no indication that the decrease in NO_2 concentrations slows down after 2010. The observed reductions in nitrogen oxides differ between winter and summer and turn out to be modulated by ozone chemistry. The RIVM surface measurements show a stronger reduction in NO_x than in NO_2, accompanied by an increase in O_3 of 4–6 ppbv, which is due to diminished NO-titration following the lower NO_x emissions, especially in winter. CLASS simulations confirm that daytime O_3 increases have shifted the NO–NO_2 equilibrium more towards NO_2, explaining the weaker reductions in NO_2 (−30%) than in NO_x (−40%) concentrations over time. The O_3 increases occur both during day and during night, and have likely shortened the NO_x lifetimes both in summer (via faster OH + NO_2+M during daytime) and in winter (via faster nighttime N_2O_5 formation and subsequent hydrolysis). Our findings suggest a reduction in anthropogenic NO_x emissions of approximately 30% in the southern part of the Netherlands, and propose that interpreting satellite NO_2 trends as a proxy for trends in NO_x emissions is well-possible over a high-NO_x region, but requires careful analysis in terms of changes in the chemical regimes and NO_x lifetime.

Introduction

Anthropogenic nitrogen oxides (NO_x = NO + NO_2) are released by fuel combustion and degrade air quality. Nitrogen oxides are harmful to the human respiratory system, contribute to the production of ozone and inorganic particulate matter, and they also lead to excessive nitrogen deposition with implications for biodiversity. Since the 1980s, Europe has invested in measures to reduce NO_x emissions through European

* Corresponding author. Royal Netherlands Meteorological Institute, De Bilt, the Netherlands.
E-mail address: folkert.boersma@knmi.nl (K.F. Boersma).

https://doi.org/10.1016/j.aeaoa.2021.100104
Received 12 August 2020; Received in revised form 15 November 2020; Accepted 26 January 2021
Available online 1 February 2021

regulations and their implementation in national laws, mainly through tightening emission standards for new cars, the so-called Euro norms (e.g. EU (2008); Vestreng et al. (2009); Hooftman et al. (2018)), the implementation of low NO_x burners and the gradual replacement of coal by gas in the energy and industry sectors (e.g. Crippa et al. (2016)). Bottom-up emission inventories indicate that European NO_x emissions have decreased by 38% between 2005 and 2017 (EEA, 2019), and that emissions in the polluted Netherlands have reduced by between 32% and 39% between 2005 and 2018.

However, actual, on-road emissions from diesel vehicles and trucks turned out to be higher than suggested from the Euro-norms (De Grauwe and Weiss, 2016), and there is considerable uncertainty in inventories. Furthermore, the measured NO_2 concentrations at the surface decrease slower than the decrease in reported NO_x emissions (EEA, 2016), which has been attributed to increases in the proportion of NO_2 in the NO_x exhaust from cars (e.g. Grange et al. (2017)). At the same time, satellite records of tropospheric NO_2 columns hinted that NO_x emissions reduced strongly during 2005–2010 over Europe (e.g. Castellanos and Boersma (2012); Curier et al. (2014)) but leveled off during 2011–2014 (Miyazaki et al., 2017). Such a 'slowdown' was also found over the United States, stirring discussion on whether US NO_x emissions decreased less than reported (Jiang et al., 2018), or the relative stability of free tropospheric (background) NO_2 has dampened the decrease in tropospheric NO_2 columns (Silvern et al., 2019). Another possible explanation for leveled-off reductions may be that the NO_x lifetime in the urban emission hotspots of North America has changed (Laughner and Cohen, 2019).

Differences between trends in reported NO_x emissions and observed atmospheric NO_2 concentrations could be the result of changes in the chemical regime wherein the emissions take place. Especially in densely populated and highly industrialized areas, reductions in NO_x emissions lead to an increase of the atmospheric NO_2/NO_x ratio, because lower NO concentrations reduce the NO-titration effect on O_3 (Itano et al. (2007); Keuken et al. (2009); Gualtieri et al. (2014); Akimoto et al. (2015)), especially in winter when VOC concentrations are low:

$$O_3 + NO \rightarrow NO_2 + O_2 \quad \text{(R1)}$$

Also the chemical lifetime of NO_x may change over time (and space) because of changes in the chemical regime. Under high-NO_x conditions, HO_x concentrations increase with decreasing NO_x emissions, resulting in faster daytime loss of NO_x itself through the $NO_2 + OH \xrightarrow{M} HNO_3$ reaction (Stavrakou et al. (2008); Valin et al. (2011); Lu and Streets (2012)). This mechanism could lead to faster reductions in satellite-observed NO_2 and surface-monitored NO_2 and NO_x concentrations than in the NO_x emissions themselves. Faster nighttime conversion of NO_x into N_2O_5 (via higher O_3 concentrations) has been hypothesized to explain the recent stronger-than-predicted NO_2 reductions over China in wintertime (Shah et al., 2020). In both the daytime and nighttime mechanisms, O_3 increases lead to decreases in lifetime: in the sunlit day as a precursor for the production of OH, and at night as the main oxidant for converting NO_x into N_2O_5, which hydrolyzes in aerosols to form HNO_3.

Here we show reductions in nitrogen oxides concentrations between 2005 and 2018 over Europe and the Netherlands specifically. We use improved retrievals of tropospheric NO_2 columns observed by the Ozone Monitoring Instrument (OMI; Levelt et al. (2018)) from the long-term data record provided by the European Quality Assurance for Essential Climate Variables (QA4ECV, www.qa4ecv.eu) project (Boersma et al., 2018), and hourly measurements of NO, NO_2, and O_3 surface concentrations from more than 20 RIVM (National Institute for Public Health and the Environment) background stations in the Netherlands, provided via the open air quality portal for Europe, AirBase (EEA, 2018). We compare the observed trends in NO_2 columns and surface NO_x concentrations to the reported trends in NO_x emissions from the EMEP and TNO-MACC-III emission inventories, and use a mixed layer chemistry model (CLASS; Chemistry Land-surface Atmosphere Soil Slab (Vilà-Guerau de Arellano et al., 2015)) to evaluate how changes in the chemical regime may explain differences between the trends in the observed NO, NO_2, and O_3 concentrations.

2. Observations and model

2.1. OMI NO_2 column retrievals

We use the OMI NO_2 record generated with the QA4ECV algorithm (Boersma et al., 2018; Lorente et al., 2017; Zara et al., 2018) to investigate trends in tropospheric NO_2 columns over Europe and specifically the Netherlands, from 2005 to 2018. The OMI UV–Vis spectrometer aboard NASA's EOS Aura spacecraft measures backscattered solar radiation from the Earth in the 270–500 nm spectral range since October 2004. The EOS-Aura satellite is in an ascending Sun-synchronous polar orbit, and crosses the equator at 13:38 local time (LT). With a swath width of 2600 km and a spatial resolution of 13 × 24 km^2 (along × across track) at nadir, OMI provided daily global-coverage data on various trace gases, including NO_2, cloud, and aerosol parameters until 2007. Since 2007, a number of across-track viewing angles (or rows), mainly in eastern direction, have been partially blocked of incoming Earth radiance. For viewing angles within this so-called row anomaly (Schenkeveld et al. (2017); Zara et al. (2018)), cloud and NO_2 retrievals are of poor quality, and flagged as unreliable in the QA4ECV data product. We thus exclude the affected rows 22–53 throughout the entire 2005–2018 period, and ensure that NO_2 columns are consistently sampled under the same viewing conditions from year to year.

OMI's radiometric stability is very good. Over the period 2004–2010 the optical degradation in the visible channel was less than 2% (Boersma et al., 2011) and remains below 2% up to today (Zara et al., 2018). Schenkeveld et al. (2017) report small degradation of radiance (1–2%) and irradiance (3–8%) over the mission, and the wavelength calibration of the instrument remained stable to 0.005–0.020 nm.

The NO_2 retrieval consists of three steps, which we briefly discuss here as each step has a different impact on the overall trend in the NO_2 columns. In order of succession: (1) fitting a modeled reflectance spectrum (405–465 nm) to the satellite-measured reflectance spectrum to determine total slant column density (SCD, or N_s) (Zara et al., 2018), (2) separation of the stratospheric and tropospheric components of the SCD via data assimilation with the TM5-MP chemistry transport model (Boersma et al., 2018), and (3) converting the tropospheric SCDs into tropospheric vertical column densities (VCD, or $N_{s,trop}$) by dividing by the tropospheric air mass factor (AMF; M_{trop}). Steps (1) and (2) are strongly constrained by the OMI observations, but the calculation of the AMF in step (3) involves model assumptions, which may affect trends. The AMF depends on viewing geometry, surface albedo (5-yr OMI climatology; Kleipool et al. (2008)), retrieved cloud information (Veefkind et al., 2016), terrain height (Global Multi-resolution Terrain Elevation Data, 2010; GMTED 2010), and a priori NO_2 vertical profiles from TM5-MP at 1 ° × 1 ° resolution (Williams et al., 2017). The retrieval equation is as follows:

$$N_{v,trop} = \frac{N_s - N_{s,\,strat}}{M_{trop}} \quad (1)$$

Spectral features of NO_2 are most prominent in the spectral region between 405 and 465 nm. The instrument signal-to-noise ratio around 440 nm is such that the spectral fitting of typical differential NO_2 absorption signatures is possible for NO_2 even for clear-sky, dark scenes (e.g. Marchenko et al., 2015; Zara et al., 2018).

We generate monthly mean OMI NO_2 tropospheric columns at a 0.08 ° × 0.04 ° (longitude × latitude, 5.5 km × 4.4 km at 52°N) grid for all months between 2005 and 2018. We use an oversampling technique wherein we (monthly) average the satellite data on a standard spatial grid with a finer resolution than the size of the OMI pixel. We exclude pixels with a cloud radiance fraction greater than 0.5 as recommended (Boersma et al., 2017). Additionally, we apply a snow-cloud

differentiation scheme (when the "snow ice flag" from NISE indicates snow-ice) in order to increase the number of observations especially for the northern part of Europe during the winter months. If the scene pressure retrieved by the O_2–O_2 cloud retrieval differs by less than 2% from the surface pressure, the retrieval over snow or ice is considered to be cloud-free and not discarded (Supplementary Material section S4).

2.2. AirBase surface NO, NO_2 and O_3 observations

We use hourly measurements from the AirBase portal (EEA, 2018) to generate monthly mean station averages of NO, NO_2, and O_3 surface concentrations for the period 2005–2018. Data collected within the Air Quality e-Reporting start from 2013, and we merged these with data from AirBase v8 available for the years before 2013. AirBase instruments measure NO_2 indirectly by thermal conversion of NO_2 to NO using a heated molybdenum surface and then detecting NO by chemiluminescence after reaction with ozone. However, the molybdenum surface also converts oxidized nitrogen compounds (HNO_3, N_2O_5, alkyl nitrates, and peroxyacetyl nitrate) to NO (e.g. Grosjean and Harrison (2005)). This results in overestimations in the measured NO_2 concentrations especially when intercepting photochemically aged air (Steinbacher et al. (2007)). The overestimations are less of a concern in polluted source regions such as the Netherlands where the NO_x:NO_y ratio is very high, especially in winter, but in our comparisons with model simulations, we correct for this known interference based on CHIMERE simulations of the monthly averaged ratio of oxidized nitrogen concentrations to NO_2 following the recipe by Lamsal et al. (2008). For The Netherlands these bias corrections are a few percent in wintertime and up to about 30% in summertime (Fig. S3).

We only use observations from urban and rural background stations and exclude NO_2 measurements from urban street stations or industrial pollution sources. Urban street stations are only representative for the street canyon itself and can therefore not be compared with the spatial resolution of OMI data. Excluding these stations also avoids difficulties in the interpretation of trends observed at roadside stations, where changes in primary NO_2 emissions from road vehicles may hide the actual trends in NO_x (e.g. Carslaw and Beever (2004); Keuken et al. (2009)). Only sites with more than 50% completeness of data coverage (in a month or season) were accepted.

2.3. NO_x emission inventories

The European Monitoring and Evaluation Programme (EMEP; www.emep.int) emission inventory is based on countries reporting their emissions of main air pollutants (including NO_x), emission factors, activity data for the latest and previous years through collection of data by the Centre on Emission Inventories and Projections (CEIP; www.ceip.at). It uses sectoral emissions as reported by countries, and it is distributed at a 50 × 50 km^2 resolution. Where no or incomplete data are reported, gaps are filled with data from different models by CEIP (EMEP, 2019; Mareckova et al., 2016). Emissions data (available online at www.emep.int) are reported until 2017[1] as national totals. Because of the detailed methodologies used in most country-specific estimates and their national focus, the reported emissions provide the most accurate bottom-up estimate for a country. However, the quality of these official emissions varies across Europe, because of discrepancies in the partitioning of emissions over sectors, sudden jumps in emission strength, and missing data for certain years.

As an alternative to these official emissions, we also use the science-based TNO-MACC-III emission inventory at a resolution of 0.0625 ° × 0.125 ° (latitude × longitude) developed by TNO (Netherlands Organization for Applied Scientific Research) for the MACC European Research Project for years 2000–2011 and a corresponding data set for 2015 (Kuenen et al., 2014, 2015). TNO-MACC-III is the successor of TNO-MACC-II and is based on EMEP emission national totals at the source sector level. Where necessary, gaps and unreliable data were replaced by emissions estimated from the IIASA-GAINS (International Institute for Applied Systems Analysis – Greenhouse Gas and Air Pollution Interactions and Synergies) mode (IIASA, 2012), the EDGAR (Emission Database for Global Atmospheric Research) inventory (Crippa et al., 2018) or TNO's default emission database, which are bottom-up emission inventories based on activity data. TNO-MACC-III and EMEP inventories are therefore not independent and partly rely on the same data. An important difference between the EMEP and TNO-MACC-III inventory is that the latter invested in more consistency in the time series, provides temporal emission profiles to break down annual emissions and a much higher resolution of the gridded data which is important to see NO_x gradients in the emissions.

2.4. CLASS model

We use the Chemistry Land-surface Atmosphere Soil Slab (CLASS) model (van Stratum et al., 2012) to simulate the chemistry of nitrogen oxides and ozone in the polluted boundary layer, accounting for dynamical processes such as entrainment of air from the free troposphere, horizontal transport, and boundary layer growth. The daytime development of the boundary layer is driven by surface latent and sensible heat fluxes (depending on soil properties and incoming solar radiation) and entrainment of air from the free troposphere, leading to a well-mixed layer with very little vertical gradient for the meteorological and chemical variables within the boundary layer. CLASS is thus a box model that simulates mean mixing ratios in the turbulent boundary layer during well-mixed conditions (van Stratum et al., 2012).

CLASS uses an O_x-NO_x-VOC-HO_x photochemistry scheme with 15 reactive species (22 in total) and 28 reactions, including relevant nighttime reactions such as the formation of N_2O_5, and subsequent conversion to HNO_3 (Vilà-Guerau de Arellano et al., 2009). This is a simplified scheme that includes isoprene and its main oxidation products, but omits some other important organic species and aerosols (the nighttime uptake of N_2O_5 on aerosols is simplified as $N_2O_5 + H_2O \rightarrow 2\,HNO_3$) (Ouwersloot et al., 2012). Nevertheless, CLASS has been shown to reproduce the observed diurnal variability and mixing ratios of the main reactants in polluted environments ranging from the Amazon to Paris (e.g. Vilà-Guerau de Arellano et al. (2009); van Stratum et al. (2012); Lorente et al. (2019)). The main advantage of using CLASS over a CTM is that it is computationally not very demanding, while still reproducing air pollution in polluted environments quite well, as shown in the above papers, and in Table 1 and Table 2 below.

The settings in CLASS were selected such that they optimally reproduce the observed ensemble mean concentrations for the southern Netherlands for winter and summer 2005 and 2018. The CLASS simulations start upon sunrise, and as initial conditions we took the observed average surface concentrations from all AirBase stations in the region at

Table 1
Mean winter-summer ratios of NO_2 concentrations at 13:00–14:00 h LT over the southern Netherlands. Winter months: December–March, Summer months: May–September. We calculated the CLASS NO_2 column by vertically integrating the CLASS NO_2 concentrations to the height of the boundary layer. Simulations done under clear-sky assumptions.

Winter-summer ratio of NO_2 concentrations	AirBase surface NO_2	CLASS boundary layer NO_2	CLASS NO_2 column	OMI column NO_2
2005	3.2	3.1	1.7	1.5
2018	3.5	3.3	1.8	1.7

[1] Since 2017 countries-members have been officially requested to submit emission reports on a significantly finer resolution of 0.1 ° × 0.1 ° (http://www.ceip.at/). About half of the EU28 parties have submitted their gridded emission data in this new resolution.

Table 2
Comparison of observed (AirBase) and simulated (CLASS) NO_x and O_3 boundary-layer mean mixing ratios for winter 2005 and 2018. The observed mixing ratios between 7:00–8:00 h LT were used as initial conditions in the CLASS simulations. AirBase surface air concentrations at 13:00–14:00 h LT were corrected for vertical gradients (−50% for NO, −40% for NO_2) based on observed vertical distributions in Berkes et al. (2018) and Dieudonné et al. (2013). Noontime ozone levels were corrected and increased by 8 μg/m^3 (4 ppb) following Klein et al. (2017).

		Winter 2005 (ppb)	Winter 2018 (ppb)	Trend 2018–2005
AirBase 7–8 h LT	NO	3.6	2.7	−25%
	NO_2	4.5	3.8	−16%
	NO_x	8.1	6.5	−20%
	NO_2: NO_x	0.56	0.58	+4%
	O_3	11.9	13.6	+14%
AirBase 13–14 h LT	NO	5.33	2.35	−56%
	NO_2	7.97	5.85	−27%
	NO_x	13.30	8.20	−38%
	NO_2: NO_x	0.60	0.71	+18%
	O_3	18.8	22.5	+20%
CLASS 13–14 h LT	NO	4.50	2.65	−41%
	NO_2	8.80	6.22	−29%
	NO_x	13.30	8.87	−34%
	NO_2: NO_x	0.66	0.70	+6%
	O_3	18.6	22.5	+21%

7:00–8:00 h LT in winter and 6:00–7:00 h LT in summer. Soil moisture was tuned such that the mixed layer simulation reproduces a 600 m deep boundary layer at 13:00–14:00 h LT in winter, and 1150 m deep boundary layer in summer, consistent with the climatology of boundary layer depths over the Netherlands presented by Seidel et al., (2012). An important difference between the winter and summer simulation is that volatile organic compounds (VOC) emissions are substantial in summer, and absent in winter. Our idealized CLASS simulations (cloudless scenes, no meteorological differences between 2005 and 2018, same isoprene emissions) have been nudged to reproduce the AirBase NO, NO_2, and O_3 concentrations. Nudging was by regulating entrainment of O_3 from the free troposphere, and NO_x emission levels. The entrainment of O_3 was similar between the different simulations, and of little consequence to the overall results.

3. Results

3.1. Annual NO_2 trends in Europe and the Netherlands

Fig. 1 shows the 2005 and 2018 annual mean QA4ECV OMI tropospheric NO_2 columns, and their differences over Europe. The OMI data show a distinct reduction in NO_2 columns over much of Europe, but especially over the polluted hotspots, with absolute reductions up to 7 × 10^{15} molec.cm^{-2} (up to 40%) over the industrialized Po Valley, Ruhr Area, and Flanders and the Netherlands. The reductions in Europe markedly contrast the substantial increases in NO_2 columns observed over Algeria and Turkey due local growth in industrial activity and traffic (Belhout et al. (2018); EEA (2019)).

The lower right panel of Fig. 1 shows that the strongest absolute and relative reductions occur in regions that had very high NO_2 levels in 2005. Reductions are 40% in polluted hotspots with columns >10 × 10^{15} molec.cm^{-2}, but less than 20% for less polluted regions with 2005 column values below 5 × 10^{15} molec.cm^{-2}. Such reductions are much higher than the changes in NO_2 columns due to meteorological variability (Curier et al., 2014). For typical unpolluted, background regions with 2005 columns <1 × 10^{15}, we do not find reductions at all. Therefore, the lower right panel of Fig. 1 suggests that NO_2 reductions analyzed for an entire continent will indeed appear to have 'slowed down': as the background NO_2 remains unchanged, its relative contribution to the spatial mean column becomes larger as anthropogenic NO_x emissions decrease with time. Only over urban and industrialized regions with high NO_2, such as the Netherlands, Po Valley, Ruhr area, and London, the background NO_2 remains far below the high pollution levels, and trends in NO_2 will be dominated by the underlying changes in local or national anthropogenic NO_x emissions as put forward by Silvern et al. (2019).

We now zoom in on the Netherlands, where NO_2 pollution is particularly high across the country. The OMI NO_2 tropospheric vertical column density within the nation's borders show a reduction from 8.3 × 10^{15} molec.cm^{-2} in 2005 to 5.4 × 10^{15} molec.cm^{-2} in 2018, a statistically significant 30% decrease in 14 years (Fig. 2). To evaluate if the decrease is dominated by the slant columns or by the air mass factors, we also show the year-to-year changes in the normalized tropospheric slant columns and inverse air mass factors over the Netherlands. The relative trend in the tropospheric NO_2 columns follows the relative trend in the normalized slant columns ($N_{S,trop}$) (−31%), where the normalization by the geometric air mass factor (M_{geo}) removes the satellite viewing angle dependencies. There is a small negative trend (−8% over 14 years) in the inverse air mass factor (M^{-1}_{trop}), which is explained by reducing NO_x emissions in TM5-MP (Williams et al., 2017) leading to a shift in the relative vertical distribution of NO_2 to higher altitudes, and consequently higher tropospheric AMFs (e.g. Boersma et al. (2004)). The geometric AMF shows no overall trend, suggesting that data sampling has not had a strong influence on the long-term trend in tropospheric NO_2 columns. The geometric and tropospheric AMFs however do show interannual variability, especially in 2010–2012, which is reflected in variability in the vertical and slant NO_2 columns, suggesting that data sampling (influenced by rejection of cloudy data, variability in meteorology (Boersma et al., 2016)) is relevant in studying trends in satellite data (Supplementary Material section 2).

Fig. 3 shows the spatial distribution of annual mean OMI tropospheric NO_2 columns and surface NO_2 concentrations (μg m^{-3}) from 23 AirBase ground stations within the Netherlands in 2005 and 2018. Both OMI and AirBase show substantial reductions in NO_2, with the strongest decreases in the southern, industrialized part of the country. To test the spatial representativeness of the locations of the 23 surface stations for the entire country, we evaluated the agreement between the nationwide-averaged and the 23-station averaged collocated monthly mean OMI NO_2 columns. The right panel of Fig. 3 shows a strong agreement ($r^2 = 0.96$) between national means and superstation means, suggesting that the spatial distribution of the 23 surface stations in the Netherlands indeed captures the nation's regional and urban background NO_2 pollution levels. The spatial correlation between OMI and ground-based NO_2 observations is not as strong, but still good in 2005 and 2018 (r^2 = 0.5–0.6, not shown) over the Netherlands.

Fig. 4 shows the time series of the annual mean OMI NO_2 columns and surface NO_2 concentrations over the Netherlands, together with trends in reported NO_x emissions. In spite of the differences in metrics and sampling techniques, the observed NO_2 and reported NO_x emissions show similar decreases: between 2005 and 2018 OMI NO_2 has reduced by 30% (−2.2 ± 0.5% yr^{-1}, Table S1), surface NO_2 by 32% (−2.6 ± 0.2% yr^{-1}), and anthropogenic NO_x emissions by 32% (TNO-MACC-III inventory) or 39% (EMEP inventory). The observed NO_2 does not point at a pronounced slowdown in NO_2 reductions after 2010 over the Netherlands such as reported over the United States (Jiang et al., 2018). Nitrate (NO_3^-) wet deposition measurements from 8 to 11 RIVM stations distributed over the Netherlands (van der Swaluw et al., 2011) also show a steady decrease over the country, with 2018 wet deposition fluxes 38% below 2005 levels (Fig. S2, Table S1). Wet deposition measurements are sampling the periods of time when OMI is not sampling (i.e. precipitation versus clear skies, by definition complementary datasets). The

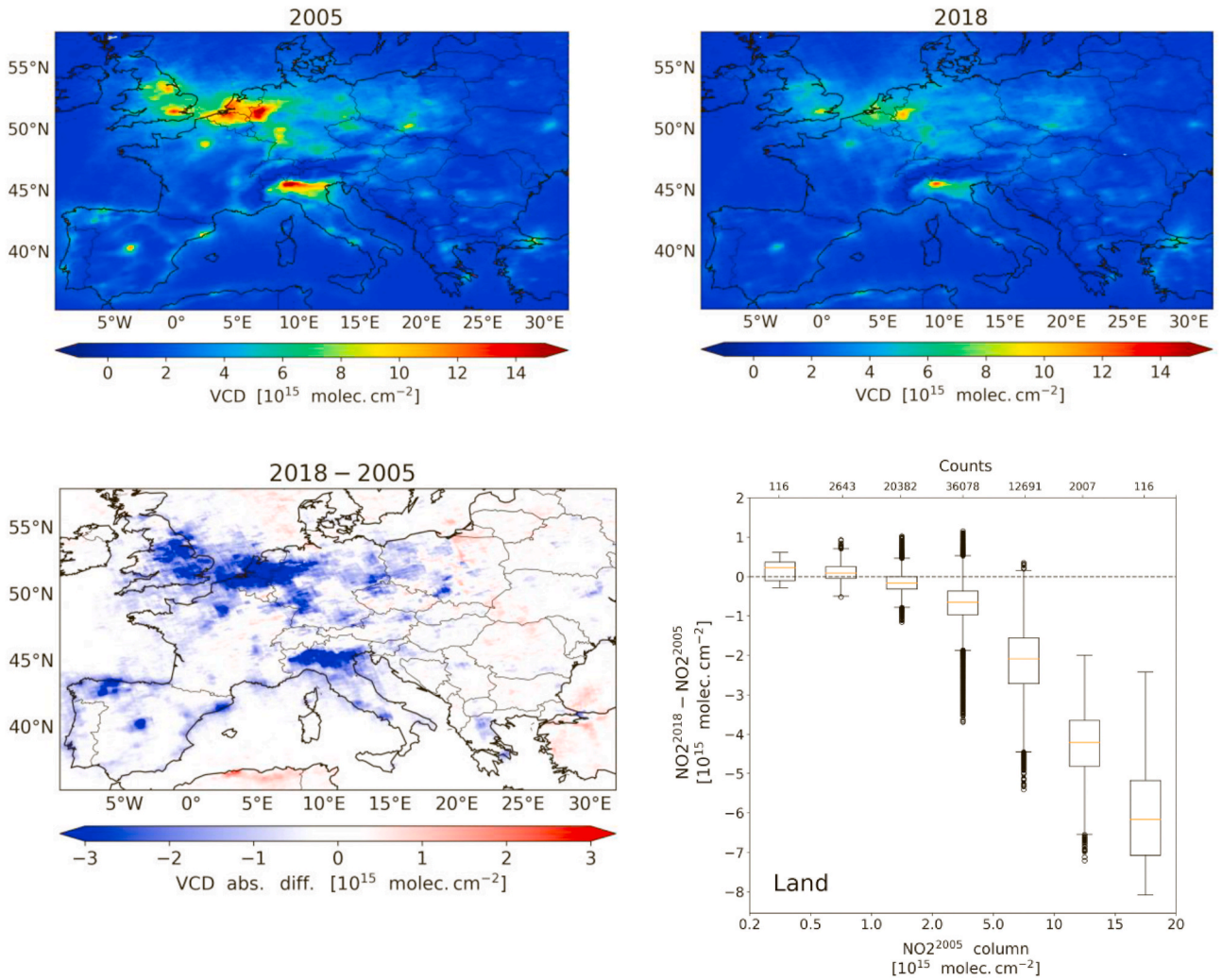

Fig. 1. Gridded (0.08 ° × 0.04 °) annual mean OMI tropospheric NO_2 columns in 2005 and 2018 (top panels) observed under mostly clear-sky situations at 13:30 h local time. The lower left panel shows the absolute differences between retrieved NO_2 columns in 2018 and 2005. The lower right panel shows a box-whisker (the box delimits the 25th and 75th percentile, and the open circles show the outliers) plot of the absolute differences between 2018 and 2005 for all grid cells over land in western Europe binned by their NO_2 column value in 2005. The upper x-axis indicates the number of grid cells that fall into each bin.

statistically significant decrease in nitrate wet deposition (−2.7 ± 0.4%/yr) reflects the decrease in NO_x emissions amplified by a reduction in precipitation of 15%–20% at the location of the stations between 2005 and 2018.

Throughout 2005–2018 surface NO_2 followed a more evenly paced reduction than shown in the OMI record. The stronger interannual variability in the satellite data can be explained by AMF variability due to temporal sampling differences related to cloud cover (Fig. 2 and Fig. S3). Another sampling difference is that the satellite trends are based on (mostly) clear-sky scenes, whereas surface station trends are based on data sampled under all-sky conditions. A sensitivity test for one Rotterdam AirBase station (Rotterdam-Schiedamsevaart, NL00418) suggests that surface NO_2 reductions appear somewhat stronger when sampled under clear-sky conditions compared to all-sky conditions, and this may partly explain the stronger reductions in the clear-sky sampled OMI data than in the all-sky sampled surface data (Fig. S4). Overall, there is good consistency (agreement within 5–10%) between the different sampling techniques.

Both the EMEP and TNO-MACC-III inventories report significant reductions in Dutch anthropogenic NO_x emissions between 2005 and 2018 (TNO-MACC-III emissions were interpolated between 2011 and 2015 and extrapolated after 2015, EMEP extrapolated for 2018). The largest emission reductions occurred in the energy sector (production and industrial use: 46%) in response to advanced combustion modification technologies (e.g. use of low NO_x burners), implementation of flue-gas abatement techniques (e.g. NO_x scrubbers and catalytic and non-catalytic reduction techniques) and fuel switching from coal to gas. Strong reductions have also been reported for the road transport sector (−41%) because of catalysts fitted to petrol-fueled vehicles and stricter emission limits for cars, and in the household sector (−40%). No NO_x emission reductions have been reported for agriculture (EEA, 2019). The reduction in the TNO inventory is less steep after 2011 (−2.4% yr^{-1}) than in EMEP (−3.2% yr^{-1}), which is probably mostly due to differences in the reporting year which can introduce adjustments upward or downward due to new insights or choices in emission factors (see section S8 in the Supplement).

3.2. Spatial differences in NO_2 trends over the Netherlands

To examine the importance of background NO_2 (Silvern et al., 2019), we separate the observations into an urban and rural regime. Fig. 3 shows that NO_2 pollution levels in the more urbanized and industrialized southern half of the Netherlands are substantially higher than in the northern half. We therefore split the Dutch domain in a southern (urban) and a northern (rural) part, using the line from IJmuiden (west of Amsterdam at the coast) to Arnhem (at the German border) as separator.

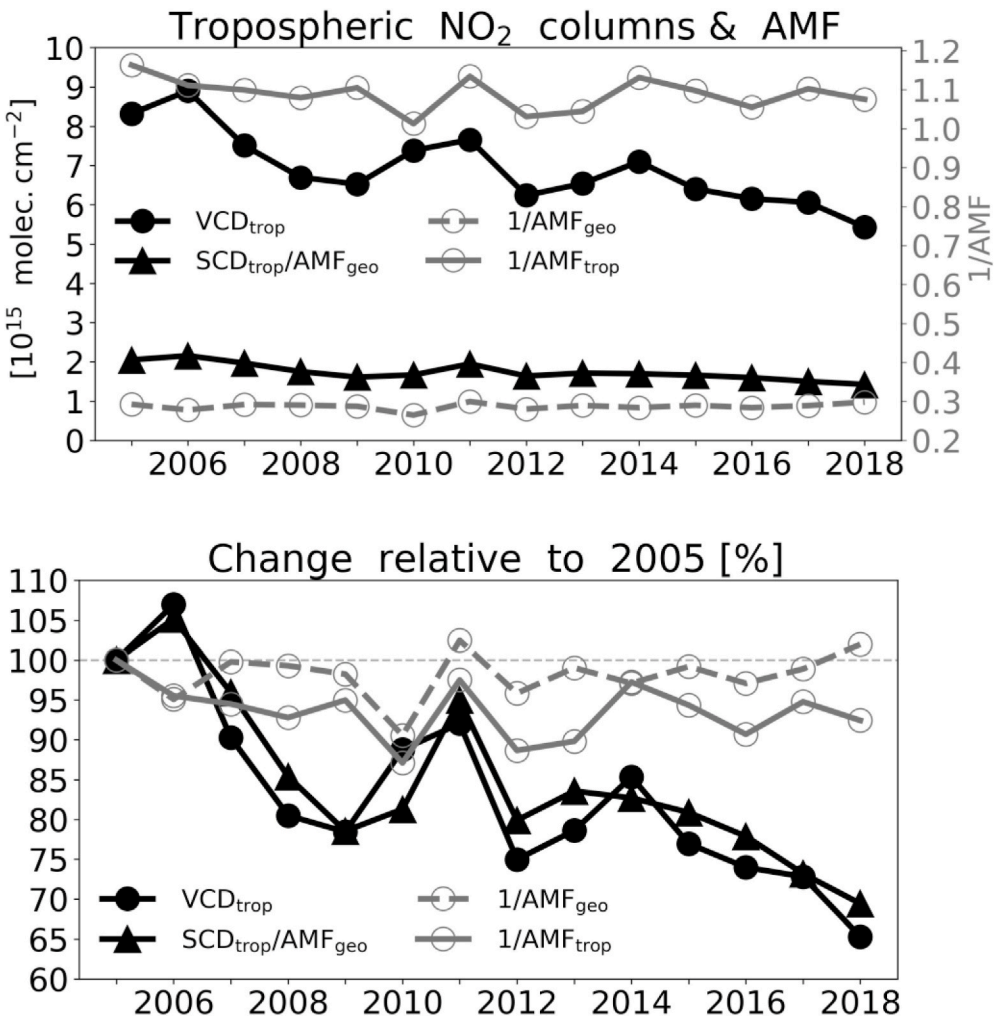

Fig. 2. (a) Time series of annual average OMI NO_2 tropospheric vertical columns (black circles), geometry-corrected OMI NO_2 tropospheric slant columns (black triangles), inverse tropospheric air mass factor (solid grey line), and the inverse geometric AMF (dashed grey line) over the Netherlands between 2005 and 2018. (b) as (a) but expressed as change relative to 2005.

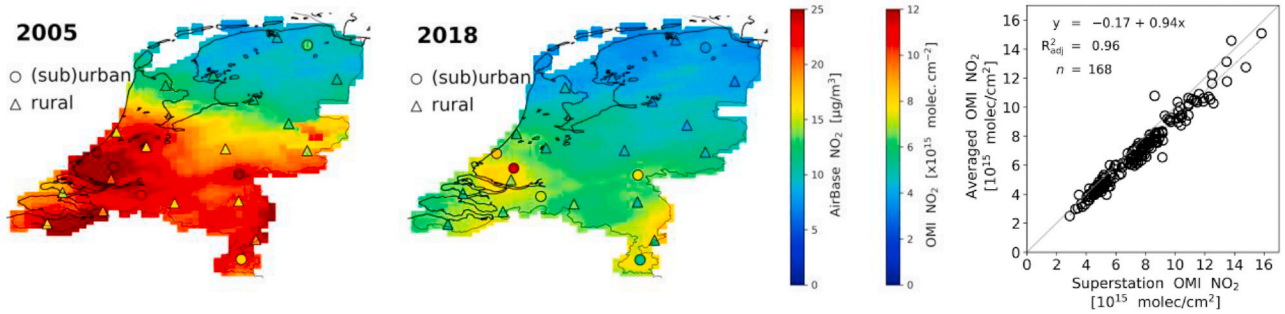

Fig. 3. Annual mean OMI NO_2 columns (0.08 ° × 0.04 ° lon × lat) and annual mean surface NO_2 concentrations at 23 rural and urban background ground stations over the Netherlands in 2005 and 2018. The circles indicate urban background and triangles indicate rural background stations according to the AirBase classification. Right panel: scatterplot of the monthly means of OMI NO_2 columns averaged over the whole country of the Netherlands and the OMI NO_2 columns averaged over the 23 grid cells collocated with the Airbase stations for the 2005–2018 period (n = 168, 14 years × 12 months).

In 2005, column NO_2 levels in the southern Netherlands were 70–75% higher than in the northern part (10.7×10^{15} molec.cm^{-2} vs. 6.1×10^{15} molec.cm^{-2}). Background NO_2 columns in models are typically 0.5–1.0 $\times 10^{15}$ molec.cm^{-2} i.e. 5-20% of the tropospheric column. Trends in the NO_2 satellite data are therefore expected to be smaller in the rural north of the country than in the urban south. In the northern part constant agricultural emissions and the relative contribution of background (free tropospheric) NO_2 are becoming proportionally more important. This is already illustrated by Fig. 1, which shows that the 2005–2018 reductions are strongest (−40%) for the most polluted regions, where the background is only a small fraction of the column. Less polluted regions, such as the north, show smaller reductions (−20%), because the larger background fraction is dampening the relative reductions there.

Fig. 5 confirms that OMI NO_2 columns over the urban (southern)

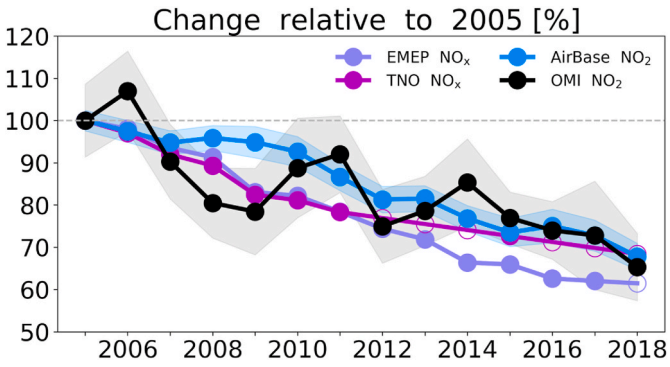

Fig. 4. Relative trends of annual mean OMI NO_2 columns (black), surface NO_2 concentrations at AirBase measurement stations (blue), TNO NO_x reported emissions (purple), and EMEP NO_x reported emissions (lila) for the 2005–2018 period over the Netherlands (2005 = 100). For years without an emission estimate available, data were linearly interpolated or extrapolated (open circles). The shaded area shows the standard error of the annual (12-month) mean estimates. (For interpretation of the references to colour in this figure legend, the reader is referred to the Web version of this article.)

Netherlands has decreased by 37% ($-2.8 \pm 0.4\%$ yr^{-1}), whereas the rural north shows a significantly weaker reduction of 18% ($-1.3 \pm 0.6\%$ yr^{-1}) between 2018 and 2005. The surface NO_2 trends (with little sensitivity to free tropospheric NO_2) are also somewhat stronger in the urban south (−33%, $-2.6 \pm 0.2\%$ yr^{-1}) than in the rural north (−29%, $-2.2 \pm 0.2\%$ yr^{-1}), providing some support to the hypothesis by Silvern et al. (2019) that the flatter OMI NO_2 trend over rural areas is due to the increasing relative importance of the background NO_2, rather than to flattening of the anthropogenic NO_x emissions over this area.

Background NO_2 (in models) is similar between Europe and the United States, so dampening effects should be anticipated in both continents. The flattening of NO_2 column trends over the Netherlands will however be less prominent than on a continental scale, as the Dutch rural areas still have high anthropogenic NO_2 levels compared to those over all of Europe (Fig. 1) or the United States (Silvern et al., 2019). Another factor that affects the response of atmospheric NO_2 concentrations to changes in NO_x emissions is a possible change in chemical regime.

3.3. *Winter and summer NO_2 trends over the Netherlands*

We now analyze differences in NO_2 between winter and summer, which are characterized by different photochemical regimes. In winter, with short days and frequently overcast skies in The Netherlands, high NO_x emissions are mixed throughout a relatively shallow boundary layer (400–600 m, Seidel et al. (2012)), and combined with low HO_x concentrations and a corresponding longer (daytime) chemical lifetime for NO_x, this results in higher NO_2 concentrations. In summertime, more vertical mixing in a deeper boundary layer (1000–1200 m, Seidel et al. (2012)) and shorter NO_x lifetimes, are leading to lower surface concentrations and tropospheric columns.

Table 1 compares the mean winter-summer ratios of the OMI NO_2 columns with the mean ratios of 13:00–14:00 h LT surface NO_2 at the 15 AirBase stations within the southern (urban) Netherlands, using CLASS simulations (model settings are in Supplemental Material) to connect boundary layer columns with concentrations. We find that the seasonal amplitudes between the AirBase data (3.2–3.4) and CLASS simulations (3.1–3.3) are consistent, once the AirBase summertime data have been corrected for the well-known molybdenum interference (30%, Supplementary Material section 4). Also the seasonal amplitudes between the OMI and CLASS NO_2 boundary layer columns are consistent (OMI: 1.5–1.7, CLASS: 1.7–1.8). The winter-to-summer ratio is much higher at the surface than the column ratio, because the column ratio accounts for the difference in boundary layer height between winter (~600 m) and summer (~1150 m) in the Netherlands.

Fig. 6 shows the observed changes in surface air (13:00–14:00 h local time) mixing ratios (ppb) of NO, NO_2, NO_x, and changes in NO_2/NO_x (ppb/ppb) in the southern Netherlands for winter and summer. There is a strong decrease in surface NO_x in both seasons between 2005 and 2018 (−38% in winter and −37% in summer, corresponding to $-3.1 \pm 0.7\%$ yr^{-1} and $-2.9 \pm 0.5\%$ yr^{-1}, respectively, see trend analysis in Table S1) in line with the magnitude of the annual average NO_x emission reductions (TNO: 2.5% yr^{-1} and EMEP: 3% yr^{-1}), but the reductions are less pronounced in NO_2 (−28%) than in NO (−51%), especially in winter. This translates as a remarkable increase in the NO_2:NO_x ratio from 0.69 (±0.04) to 0.78 (±0.03) between 2005 and 2018 in winter, and from 0.77 (±0.02) to 0.83 (±0.07) in summer: a larger portion of NO_x is NO_2 in 2018 than it was in 2005. At the same time, O_3 has increased significantly by 0.3 ± 0.1 ppb yr^{-1} between the 2005 and 2018 winters and by 0.2 ± 0.2 ppb yr^{-1}, an insignificant increase (Table S1) between the 2005 and 2018 summers in the southern Netherlands (Fig. 7(a)). Such increases in urban and suburban O_3 have also been reported elsewhere in Europe (Yan et al., 2018). The observed increase in O_3 reflects at least partly the reduced NO-titration by the $O_3 + NO \rightarrow NO_2 + O_2$ reaction (R1) as emissions decreased.

To evaluate the origin of the observed increases in ozone, we use the concept of "odd oxygen" (Sillman, 1999) or "total ozone" (Chou et al., 2006). "Odd oxygen" or "Total ozone" is defined as $[O_3]+[NO_2]$ representing the net photochemically produced O_3 plus O_3 transported into the area including the effect of the local reduction of O_3 by NO titration via R1 (every NO consuming O_3 turns into a NO_2 molecule). If total ozone stays constant over time, the O_3 increase and the enhanced NO_2:NO_x ratio are the result of the reduced titration from NO, and cannot be explained by photochemical production or increased inflow of O_3. If total ozone increases over time, then the O_3 increase is also due to stronger photochemical production or increased inflow. Fig. 7(a) and (b) show the timeseries of total ozone over the southern part of the Netherlands for winter and summer. In winter, there is no increase in

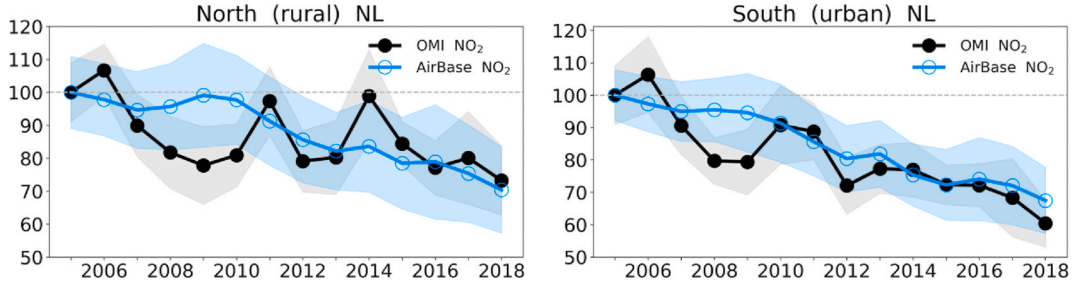

Fig. 5. Time series of annual mean OMI NO_2 columns (black) and AirBase NO_2 concentrations (blue) for the northern ("rural") and the southern ("urban") Netherlands as divided by the straight line that connects IJmuiden [4.62° E, 52.69° N] and Arnhem [7.33° E, 51.38° N]. The shaded areas indicate the standard errors on the annual (12-month) mean NO_2 levels. (For interpretation of the references to colour in this figure legend, the reader is referred to the Web version of this article.)

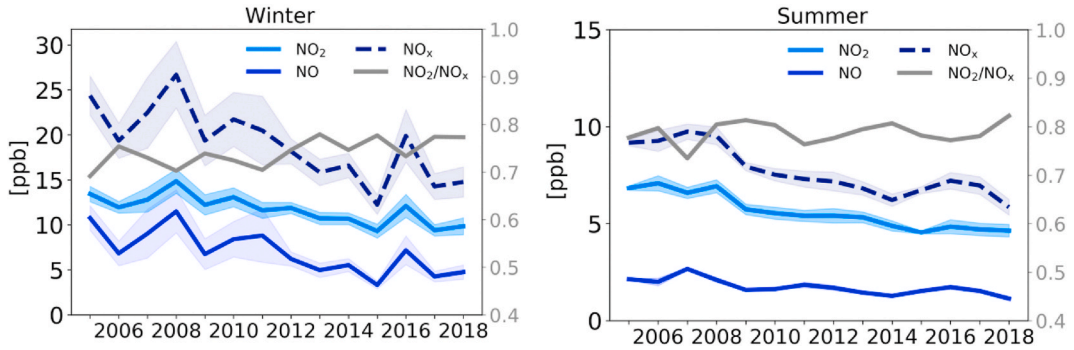

Fig. 6. Seasonally averaged mixing ratios of NO, NO_2, and NO_x in surface air (13:00–14:00 h local time), and their standard deviations (shaded), and in the NO_2:NO_x ratio in the southern part of the Netherlands for 2005–2018. Winter here is the average between December and March of the following year, and summer is the average between May and August. The dashed areas indicate the standard errors in the seasonal (4-month) means.

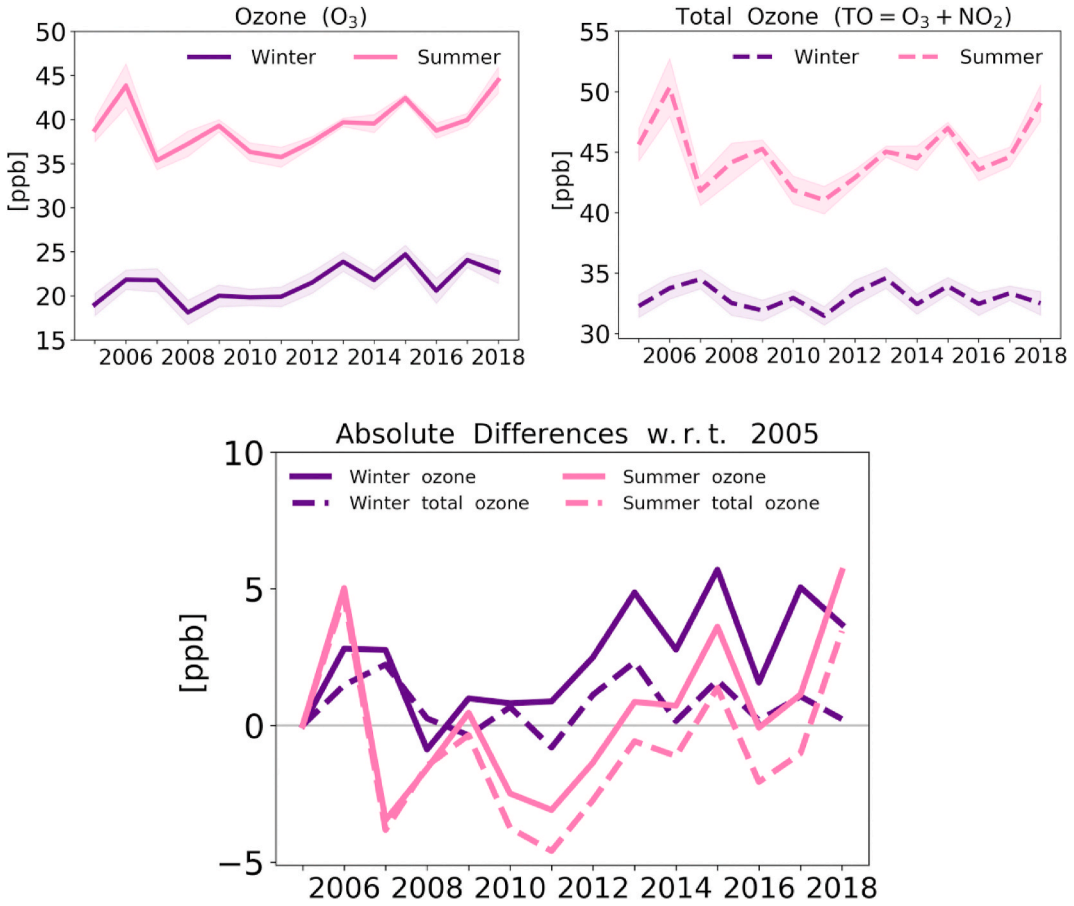

Fig. 7. Seasonally averaged changes in (a) O_3 and (b) total ozone ($[O_3]+[NO_2]$) (and their standard deviations, 13:00–14:00 h local time) between 2005 and 2018 in the southern part of the Netherlands. Shaded areas indicate the standard error on the seasonal (4-month) means. (c) Absolute increase in O_3 and total ozone relative to the 2005 seasonal averages.

total ozone between 2005 and 2018 ($0.0 \pm 0.2\%$ yr^{-1}, Table S1): the O_3 increase is exclusively due to the reduced titration from NO. In summer, the increase in total ozone is < 3.5 ppb, but the trend is insignificant ($0.1 \pm 0.4\%$ yr^{-1}, Table S1) while the increase in O_3 was 5.7 ppb, suggesting that one third of the summertime ozone increase is caused by reduced titration.

3.4. Interpretation of winter and summer NO_2 trends with CLASS

To evaluate possible changes in the chemical regime in which the decreases of NO_2 took place, we simulated NO, NO_2, HNO_3, O_3 and OH concentrations in the boundary layer with the CLASS model over the southern Netherlands. The model settings were selected such that they optimally reproduce the observed station mean concentrations for the southern Netherlands for winter and summer 2005 and 2018 (Supplementary Material section 6).

Table 2 compares the 2005 and 2018 observed and simulated mixing ratios of nitrogen oxides and ozone in the boundary layer. CLASS with 50% smaller wintertime NO_x emissions in 2018 than in 2005 captures the reductions in nitrogen oxides and increase in O_3 concentrations reasonably well, confirming that NO_x reductions (−34%) are stronger than NO_2 reductions (−29%), and also showing larger NO_2:NO_x ratios in

2018 than 2005, albeit less strong than observed (Fig. 6(a)). The CLASS simulations suggest that the increase in the NO_2:NO_x ratio can indeed be understood from the changes in the photochemical steady state between NO, NO_2 and O_3. With O_3 increasing due to reduced NO-titration, the equilibrium between NO and NO_2 shifts more towards NO_2, dampening the reductions in NO_2 over time. We estimate that the OMI wintertime NO_2 reduction of 30% therefore reflects a reduction in atmospheric NO_x of 34% (based on CLASS-simulated trends in NO_2:NO_x) to 41% (based on AirBase NO_2:NO_x at the surface) over the southern Netherlands between 2005 and 2018 (Fig. 8(a)).

In summer, CLASS (with 2018 emissions 15% lower than in 2005) also simulates somewhat stronger reductions in NO_x (−41%) than in NO_2 (−37%), as shown in Table 3. Again, we see an increase in the NO_2:NO_x ratio, but not as pronounced as in winter because of the higher summertime photolysis rates. Considering the slight increase in the NO_2:NO_x ratio over time, the observed OMI summertime NO_2 reduction of 38% would represent a slightly stronger reduction in NO_x of between 41% and 42% (based on the CLASS-simulated or AirBase-observed increases in the NO_2:NO_x ratio) (Fig. 8(b)).

Based on the above analysis of simulated and observed changes in the NO_2:NO_x ratios, we conclude that the OMI NO_2 reductions of 30–38% between 2018 and 2005 over the highly polluted southern Netherlands do not fully reflect the more pronounced underlying reductions in NO_x concentrations, which we estimate to be in the range of 34%–42%. We anticipate that in other high-NO_x regions in western Europe, such as London, Paris, and the Ruhr area, similar effects will be seen.

3.5. Possible implications for NO_x lifetime

The long-term increase in O_3 suggests that the Dutch lower atmosphere has become more oxidative, and this can shorten the chemical lifetime of NO_x. In daytime and in summer, long-term increases in O_3 are positively correlated with increases in OH (e.g. Monks et al. (2015)), the main daytime sink for NO_x. This mechanism is expected to lead to a reduction in the (daytime) NO_x lifetime in summer but not in winter, when OH levels are very low. At night, long-term increases in O_3 also speed up the NO_x loss. Higher nighttime O_3 levels promote the conversion of NO_x into N_2O_5, which then reacts in aerosols to produce HNO_3 (e.g. Kenagy et al. (2018); Shah et al. (2020)).

Our CLASS simulations for winter and summer provide the opportunity to evaluate how the lifetime of NO_x changed between 2005 and 2018 in the southern Netherlands. The simulations are initiated and constrained by the observed NO, NO_2, and O_3 mixing ratios in the

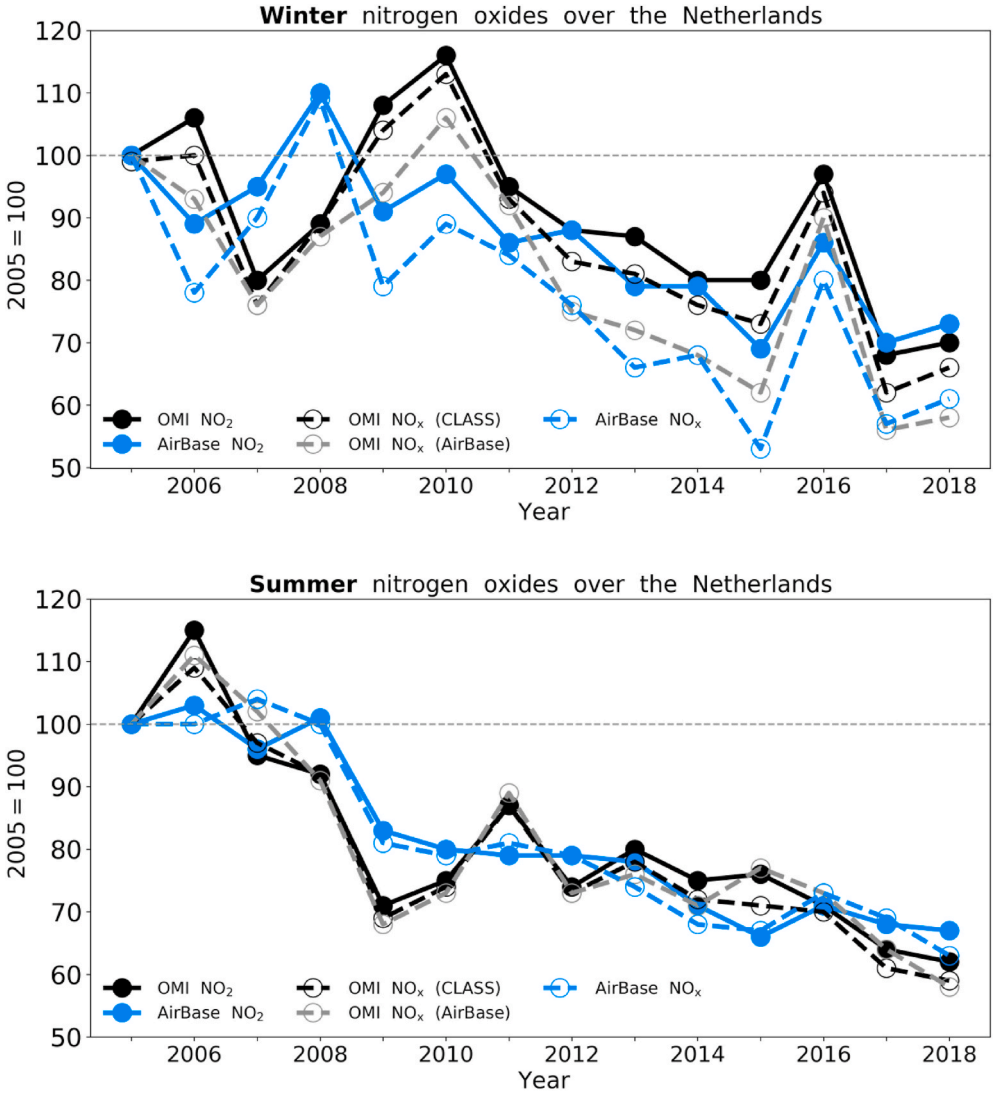

Fig. 8. Relative changes in OMI NO_2 columns and AirBase (boundary layer mean) NO_2 mixing ratios (13:00–14:00 h local time) between 2005 and 2018 over the southern part of the Netherlands in winter (upper panel) and summer (bottom panel). The OMI NO_x changes have been inferred from the simulated (CLASS) and observed (AirBase) NO_2:NO_x ratios.

Table 3
Comparison of observed (AirBase) and simulated (CLASS) NO_x and O_3 boundary-layer mean mixing ratios for summer 2005 and 2018. The observed mixing ratios between 6:00–7:00 h LT were used as initial conditions in the CLASS simulations. AirBase surface air concentrations were corrected for vertical gradients (−50% for NO, −40% for NO_2) based on observed vertical distributions in Berkes et al. (2018) and Dieudonné et al. (2013). No vertical correction was applied to ozone.

		Summer 2005 (ppb)	Summer 2018 (ppb)	Trend 2018–2005
AirBase 6–7 h LT	NO	1.90	1.25	−34%
	NO_2	3.61	3.07	−15%
	NO_x	5.51	4.32	−22%
	NO_2:NO_x	0.66	0.71	+8%
	O_3	15.2	20.5	+35%
AirBase 13–14 h LT	NO	1.10	0.58	−47%
	NO_2	2.73	1.85	−32%
	NO_x	3.83	2.43	−37%
	NO_2:NO_x	0.71	0.76	+7%
	O_3	39.8	45.6	+15%
CLASS 13–14 h LT	NO	1.33	0.68	−49%
	NO_2	2.71	1.71	−37%
	NO_x	4.04	2.39	−41%
	NO_2:NO_x	0.67	0.70	+5%
	O_3	39.7	45.6	+15%

southern Netherlands in 2005 and 2018 (Tables 2 and 3). The 2005 and 2018 simulations were identical in terms of meteorology and isoprene emissions, but different in initial conditions and NO_x emissions. We evaluated the NO_x lifetime in the boundary layer as:

$$\overline{\tau_{24}} = \frac{\left[\overline{NO_x}\right]}{P_{HNO_3}} \quad (2)$$

with $[\overline{NO_x}]$ the 24-h averaged NO_x mixing ratio and P_{HNO_3} the simulated nitric acid production rate in the CLASS model over the period of 24 h.

Table 4 shows that the winter lifetime decreased from 25 to 19 h (−23%) between 2005 and 2018. Despite lower NO_x levels in 2018 than in 2005, HNO_3 concentrations increased, especially at night (2005: 8.2 ppb, 2018: 8.8 ppb). The daytime NO_x conversion to HNO_3 was as small in 2005 as in 2018. As suggested by Shah et al. (2020), the most likely driver for the faster nighttime loss of NO_x given our basic description of nighttime chemistry is an increase in nighttime O_3 levels in the stable boundary layer. Through the NO + O_3 and NO_2+O_3 reactions O_3 promotes the formation of N_2O_5 and subsequent hydrolysis. Nighttime O_3 in The Netherlands has indeed increased by ~2 ppb (see Table 2) between 2005 and 2018. In summer, we find a decrease in lifetime from 9 to 8 h (−11%) as daytime OH increased by 9% from 0.39 ppq to 0.42 ppq, and nighttime O_3 increased by 5 ppb (Table 2), leading to faster nighttime HNO_3 formation as in winter.

Table 4
CLASS-simulated 24-h mean NOx concentration, HNO_3 production and NO_x lifetime for the winters and summers of 2005 and 2018. The CLASS simulations were constrained by the observed (AirBase) NO, NO_2 and O_3 mixing ratios averaged over all stations in the southern Netherlands.

		Winter 2005	Winter 2018	Trend
24-h mean	$[NO_x]$	9.2 ppb	7.5 ppb	−19%
24-h mean	P_{HNO_3}	8.8 ppb/day	9.2 ppb/day	+6%
24-h mean	$\overline{\tau_{24}}$	25.1 h	19.3 h	−23%
		Summer 2005	Summer 2018	Trend
24-h mean	$[NO_x]$	3.6 ppb	2.7 ppb	−25%
24-h mean	P_{HNO_3}	9.6 ppb/day	8.1 ppb/day	−16%
24-h mean	$\overline{\tau_{24}}$	9.0 h	8.0 h	−11%

The implications of the changes in lifetime for NO_x emissions estimates in The Netherlands are difficult to evaluate without a formal chemistry-transport model-based inversion scheme (Visser et al., 2019). With such a scheme, the variable influence of meteorology on the relationship between local NO_x emissions and concentrations can be assessed. Still, the observed increases in O_3 signify a shortening of the wintertime NO_x lifetime, so that wintertime NO_x emissions may not have changed as much as the concentration reductions suggest (−38%). In summer, there is a smaller change in NO_x lifetime and the changes in NO_x concentrations and NO_2 columns should be a reliable tracker of NO_x emission changes, which we estimate to have decreased by 30–40% between 2005 and 2018. Our findings are in line with the Netherlands transitioning to a more NO_x-limited regime (Jin et al., 2017), and suggest that the TNO-MACC-III predicted emission reductions are in better agreement with the observed changes in NO_x and the chemical regime than the EMEP-predicted emissions. Both inventories mostly rely on similar data for the Netherlands, but EMEP data were from a more recent reporting year. This suggests that in recent years the reporting of NO_x emission reductions may be on the optimistic side in terms of efficiency of implemented measures as our results indicate a somewhat slower pace than the EMEP inventory suggests.

Conclusions

We examined how nitrogen oxides concentrations over The Netherlands have changed between 2005 and 2018. We find that tropospheric NO_2 columns derived from OMI have reduced by 30% throughout the country, in line with a 32% reduction in surface NO_2 concentrations observed at 23 rural and urban background stations in the Netherlands, and with two European emission inventories in which Dutch NO_x emissions have decreased by 32% and 39% in that period. OMI NO_2 shows considerable variability from year to year, compared to more gradual changes observed on the ground. This is likely due to infrequent sampling of OMI especially in the winter season when cloud cover is high. OMI NO_2 columns fall off faster in the densely populated and highly polluted south (−37%) than in the more rural northern Netherlands (−18%), suggesting a dampening influence of background NO_2 on the trends in the north. The observations do not provide evidence for a slowdown in NO_2 reductions after 2010 in the southern part of the Netherlands. We analyzed trends in winter and summer, which are characterized by very different photochemical regimes in The Netherlands. In winter we find 3 times higher surface NO_2 concentrations and 1.7 times higher NO_2 columns than in summer. The CLASS chemistry model reproduces this seasonality, which can be explained by the longer NO_x chemical lifetime and shallower boundary layer depth in winter than in summer. Ozone chemistry plays an important role in the interpretation of the wintertime and summertime NO_x-trends: surface measurements show a stronger reduction in NO_x than in NO_2, accompanied by a long-term increase in O_3. In winter, the O_3 increase of 4 ppb is exclusively due to the reduced NO-titration in response to lower emissions. In summer, the reduced NO-titration contributes to the long-term increase of O_3 (of 6 ppb) in the Netherlands. The CLASS model simulations explain the increase in the NO_2:NO_x ratio from the changes in the photochemical steady state between NO, NO_2 and O_3. With daytime O_3 increasing due to reduced NO-titration, the equilibrium between NO and NO_2 shifts more towards NO_2, which leads to weaker reductions in NO_2 (−30%) than in NO_x (−40%) over time. The O_3 increases occur during the day as well as at night. CLASS simulations that reproduce these changes suggest that the observed O_3 increases have led to shorter NO_x lifetimes both in summer (via faster OH + NO_2+M during daytime) and in winter (via faster nighttime N_2O_5 formation and subsequent hydrolysis (Shah et al., 2020)). Overall, our findings support a reduction

in anthropogenic NO_x emissions of approximately 30% in the southern part of the Netherlands, which is in reasonable agreement with the TNO-MACC-III emission inventory.

Data availability

Daily and monthly mean QA4ECV NO_2 data from OMI is publicly available from www.qa4ecv.eu and www.temis.nl. The OMI NO_2 dataset is linked to a digital object identifier (DOI) (http://doi.org/10.21944/qa4ecv-no2-omi-v1.1, Boersma et al. (2017)). Surface NO_x and O_3 concentrations are publicly available from the AirBase portal hosted by the European Environmental Agency (https://www.eea.europa.eu/data-and-maps/data/aqereporting-8). The EMEP emission inventory are available at www.emep.int, and the inventory from TNO (TNO-MACC-III) is available on request by contacting HDvdG. The code and executable of the CLASS model can be downloaded from https://classmodel.github.io/, and CLASS start and input settings can be obtained as electronic files from the corresponding author. Nitrate wet deposition measurements over The Netherlands taken by RIVM can be obtained from EvdS upon request.

Funding

This research was supported by the EU FP7 Project Quality Assurance for Essential Climate Variables (QA4ECV), grant no. 607405.

CRediT authorship contribution statement

Marina Zara: Methodology, Software, Validation, Formal analysis, Investigation, Data curation, Writing - original draft, preparation, Visualization. **K. Folkert Boersma:** Conceptualization, Validation, Investigation, Resources, Data curation, Writing - original draft, Supervision, Project administration, Funding acquisition. **Henk Eskes:** Software, Resources, Data curation, Writing - review & editing. **Hugo Denier van der Gon:** Validation, Resources, Writing - review & editing. **Jordi Vilà-Guerau de Arellano:** Methodology, Software, Resources, Writing - review & editing. **Maarten Krol:** Methodology, Writing - review & editing. **Eric van der Swaluw:** Validation, Resources, Data curation. **William Schuch:** Validation, Resources, Data curation. **Guus J.M. Velders:** Conceptualization, Writing - review & editing.

Declaration of competing interest

The authors declare that they have no known competing financial interests or personal relationships that could have appeared to influence the work reported in this paper.

Appendix A. Supplementary data

Supplementary data to this article can be found online at https://doi.org/10.1016/j.aeaoa.2021.100104.

References

Akimoto, H., Mori, Y., Sasaki, K., Nakanishi, H., Ohizumi, T., Itano, Y., 2015. Analysis of monitoring data of ground-level ozone in Japan for long-term trend during 1990-2010: causes of temporal and spatial variation. Atmos. Environ. 102, 302–310. https://doi.org/10.1016/j.atmosenv.2014.12.001.

Belhout, D., Kerbachi, R., Relvas, H., Miranda, A.I., 2018. Air quality assessment in algiers city, air quality. Atmosphere & Health 11, 897–906. https://doi.org/10.1007/s11869-018-0589-x.

Berkes, F., Houben, N., Bundke, U., Franke, H., Pätz, H.-W., Rohrer, F., Wahner, A., Petzold, A., 2018. The IAGOS NO_x instrument – design, operation and first results from deployment aboard passenger aircraft. Atmos. Meas. Tech. 11, 3737–3757. https://doi.org/10.5194/amt-11-3737-2018.

Boersma, K.F., Eskes, H.J., Brinksma, E.J., 2004. Error Analysis for tropospheric NO_2 retrieval from space. J. Geophys. Res. 109, D04311. https://doi.org/10.1029/2003JD003962.

Boersma, K.F., Vinken, G.C.M., Eskes, H.J., 2016. Representativeness errors in comparing chemistry transport and chemistry climate models with satellite UV–Vis tropospheric column retrievals, Geosci. Model. Dev. 9, 875–898. https://doi.org/10.5194/gmd-9-875-2016.

Boersma, K.F., van Geffen, J., Eskes, H., van der A, R., De Smedt, I., Van Roozendael, M., Yu, H., Richter, A., Peters, E., Beirle, S., Wagner, T., Lorente, A., Scanlon, T., Compernolle, S., Lambert, J.-C., 2017. Product Specification Document for the QA4ECV NO_2 ECV precursor product (version 1.1). QA4ECV Deliv. 4 (6). http://temis.nl/qa4ecv/no2col/QA4ECV_NO2_PSD_v1.1.compressed.pdf.

Boersma, K.F., Eskes, H.J., Richter, A., De Smedt, I., Lorente, A., Beirle, S., van Geffen, J. H.G.M., Zara, M., Peters, E., Van Roozendael, M., Wagner, T., Maasakkers, J.D., van der A, R.J., Nightingale, J., De Rudder, A., Irie, H., Pinardi, G., Lambert, J.-C., Compernolle, S.C., 2018. Improving algorithms and uncertainty estimates for satellite NO_2 retrievals: results from the quality assurance for the essential climate variables (QA4ECV) project. Atmos. Meas. Tech. 11, 6651–6678. https://doi.org/10.5194/amt-11-6651-2018.

Carslaw, D.C., Beevers, S.D., 2004. Investigating the potential importance of primary NO_2 emissions in a street canyon. Atmos. Environ. 38, 3585. https://doi.org/10.1016/j.atmosenv.2004.03.041, 359.

Castellanos, P., Boersma, K.F., 2012. Reductions in nitrogen oxides over Europe driven by environmental policy and economic recession. Sci. Rep. 2 (265) https://doi.org/10.1038/srep00265.

Chou, C.C.-K., Liu, S.C., Lin, C.-Y., Shiu, C.-J., Chang, K.-H., 2006. The trend of surface ozone in Taipei, Taiwan, and its causes: implications for ozone control strategies. Atmos. Environ. 40, 3898–3908.

Crippa, M., Janssens-Maenhout, G., Dentener, F., Guizzardi, D., Sindelarova, K., Muntean, M., Van Dingenen, R., Granier, C., 2016. Forty years of improvements in European air quality: regional policy-industry interactions with global impacts. Atmos. Chem. Phys. 16, 3825–3841. https://doi.org/10.5194/acp-16-3825-2016.

Crippa, M., Guizzardi, D., Muntean, M., Schaaf, E., Dentener, F., van Aardenne, J.A., Monni, S., Doering, U., Olivier, J.G.J., Pagliari, V., Janssens-Maenhout, G., 2018. Gridded emissions of air pollutants for the period 1970–2012 within EDGAR v4.3.2. Earth Syst. Sci. Data 10, 1987–2013. https://doi.org/10.5194/essd-10-1987-2018.

Curier, R.L., Kranenburg, R., Segers, A.J.S., Timmermans, R.M.A., Schaap, M., 2014. Synergistic use of OMI NO_2 tropospheric columns and LOTOS-EUROS to evaluate the NO_x emission trends across Europe. Remote Sens. Environ. 149, 58–69.

Dieudonné, E., Ravetta, F., Pelon, J., Goutail, F., Pommereau, J.-P., 2013. Linking NO2 surface concentration and integrated content in the urban developed atmospheric boundary layer. Geophys. Res. Lett. 40, 1247–1251. https://doi.org/10.1002/grl.50242.

EEA, 2016. Air quality in Europe – 2016. Report. https://doi.org/10.2800/80982. ISBN 978-92-9213-847-9, last access 11 February 2020.

EEA, 2018. Air quality e-reporting. https://www.eea.europa.eu/data-and-maps/data/aqereporting-8 (last access: 20 January 2020).dataset.

EEA, 2019. National emission ceilings (NEC). Directive Report. Status 2019. https://doi.org/10.2800/49299 last access 26 February 2020.

European Union, 2008. EC Directive 2008/50/EC of the European Parliament and of the Council on 21 May 2008 on the Ambient Air Quality and Cleaner Air for Europe. Off J Eur Union, pp. 1–44.

Grange, S.K., Lewis, A.C., Moller, S.J., Carslaw, D.C., 2017. Lower vehicular primary emissions of NO_2 in Europe than assumed in policy projections. Nat. Geosci. 10, 914–918. https://doi.org/10.1038/s41561-017-0009-0.

Grosjean, D., Harrison, J., 1985. Response of chemiluminescence NO_x analyzers and ultraviolet ozone analyzers to organic air pollutants. Environ. Sci. Technol. 19, 862–865.

Gualtieri, G., Crisci, A., Tartaglia, M., Toscano, P., Vagnoli, C., Andreini, B.P., Gioli, B., 2014. Analysis of 20-year air quality trends and relationship with emission data: the case of Florence (Italy). Urban Climate 10 (3), 530–549. https://doi.org/10.1016/j.uclim.2014.03.010.

Hooftman, N., Messagie, M., Van Mierlo, J., Coosemans, T., 2018. A review of the European passenger car regulations–Real driving emissions vs local air quality. Renew. Sustain. Energy Rev. 86, 1–21. https://doi.org/10.1016/j.rser.2018.01.012.

IIASA, 2012. International Institute for applied systems analysis: GAINS detailed emissions by source and activity. https://gains.iiasa.ac.at/gains/.

Itano, Y., Bandow, H., Takenaka, N., Saitoh, Y., Asayama, A., Fukuyama, J., 2007. Impact of NO_x reduction on long-term ozone trends in an urban atmosphere. Sci. Total Environ. 379 (1), 46–55.

Jiang, Z., McDonald, B.C., Worden, H., Worden, J.R., Miyazaki, K., Qu, Z., Henze, D.K., Jones, D.B.A., Arellano, A.F., Fischer, E.V., Zhu, L., Boersma, K.F., 2018. Unexpected slowdown of US pollutant emission reduction in the past decade. Proc. Natl. Acad. Sci. Unit. States Am. 201801191. https://doi.org/10.1073/pnas.1801191115.

Jin, X., Fiore, A., Murray, L., Valin, L., Lamsal, L., Duncan, B., Boersma, K.F., De Smedt, I., González Abad, G., Chance, K., Tonnesen, G., 2017. Evaluating a space-based indicator of surface ozone-NOx-VOC sensitivity over mid-latitude source regions and application to decadal trends. J. Geophys. Res. 122 (10), 439–461. https://doi.org/10.1002/2017JD026720.

Keuken, M., Roemer, M., van den Elshout, S., 2009. Trend analysis of urban NO_2 concentrations and the importance of direct NO_2 emissions versus ozone/NO_x equilibrium. Atmos. Environ. 43, 4780–4783. https://doi.org/10.1016/j.atmosenv.2008.07.043.

Klein, A., Ancellet, G., Ravetta, F., Thomas, J.L., Pazmino, A., 2017. Characterizing the seasonal cycle and vertical structure of ozone in Paris, France using four years of ground based LIDAR measurements in the lowermost troposphere. Atmos. Environ. 167, 603–615. https://doi.org/10.1016/j.atmosenv.2017.08.016.

Kleipool, Q.L., Dobber, M.R., De Haan, J.F., Levelt, P.F., 2008. Earth surface reflectance climatology from three years of OMI data. J. Geophys. Res. https://doi.org/10.1029/2008JD010290.

Kuenen, J.J.P., Visschedijk, A.J.H., Jozwicka, M., Denier Van Der Gon, H.A.C., 2014. TNO-MACC_II emission inventory; a multi-year (2003–2009) consistent high-resolution European emission inventory for air quality modelling. Atmos. Chem. Phys. 14 (20), 10963–10976. https://doi.org/10.5194/acp-14-10963-2014.

Kuenen, J., Visschedijk, A., Denier van der Gon, H.A.C., 2015. TNO_MACC-III inventory and its application for FAIRMODE SoAp. http://fairmode.jrc.ec.europa.eu/Aveiro.

Lamsal, L.N., Martin, R.V., van Donkelaar, A., Steinbacher, M., Celarier, E.A., Bucsela, E., Dunlea, E.J., Pinto, J.P., 2008. Ground-level nitrogen dioxide concentrations inferred from the satellite-borne Ozone Monitoring Instrument. J. Geophys. Res. 113, D16308. https://doi.org/10.1029/2007JD009235.

Laughner, J.L., Cohen, R.C., 2019. Direct observation of changing NO_x lifetime in North American cities. Science 366, 723–727. https://doi.org/10.1126/science.aax6832.

Levelt, P.F., Joiner, J., Tamminen, J., Veefkind, J.P., Bhartia, P.K., Stein Zweers, D.C., Duncan, B.N., Streets, D.G., Eskes, H., van der A, R., McLinden, C., Fioletov, V., Carn, S., de Laat, J., DeLand, M., Marchenko, S., McPeters, R., Ziemke, J., Fu, D., Liu, X., Pickering, K., Apituley, A., González Abad, G., Arola, A., Boersma, F., Chan Miller, C., Chance, K., de Graaf, M., Hakkarainen, J., Hassinen, S., Ialongo, I., Kleipool, Q., Krotkov, N., Li, C., Lamsal, L., Newman, P., Nowlan, C., Suleiman, R., Tilstra, L.G., Torres, O., Wang, H., Wargan, K., 2018. The ozone monitoring instrument: overview of 14 years in space. Atmos. Chem. Phys. 18, 5699–5745. https://doi.org/10.5194/acp-18-5699-2018.

Lorente, A., Folkert Boersma, K., Yu, H., Dörner, S., Hilboll, A., Richter, A., Liu, M., Lamsal, L.N., Barkley, M., De Smedt, I., Van Roozendael, M., Wang, Y., Wagner, T., Beirle, S., Lin, J.-T., Krotkov, N., Stammes, P., Wang, P., Eskes, H.J., Krol, M., 2017. Structural uncertainty in air mass factor calculation for NO_2 and HCHO satellite retrievals. Atmos. Meas. Tech. 10, 759–782. https://doi.org/10.5194/amt-10-759-2017.

Lorente, A., Boersma, K.F., Eskes, H.J., Veefkind, J.P., van Geffen, J.H.G.M., de Zeeuw, M.B., Denier van der Gon, H.A.C., Beirle, S., Krol, M.C., 2019. Quantification of nitrogen oxides emissions from build-up of pollution over Paris with TROPOMI. Sci. Rep. 9, 20033. https://doi.org/10.1038/s41598-019-56428-5.

Lu, Z., Streets, D.G., 2012. Increase in NO_x emissions from Indian thermal power plants during 1996–2010: unit-based inventories and multisatellite observations. Environ. Sci. Technol. 46, 7463–7470. https://doi.org/10.1021/es300831w.

Mareckova, K., Pinterits, M., Tista, M., Wankmueller, R., 2016. Inventory Review 2016, Review of Emission Data Reported under the LRTAP Convention and NEC Directive, Stage 1 and 2 Review, Status of Gridded and LPS Data. EEA/CEIP Vienna.

Miyazaki, K., Eskes, H., Sudo, K., Boersma, K.F., Bowman, K., Kanaya, Y., 2017. Decadal changes in global surface NO_x emissions from multi-constituent satellite data assimilation. Atmos. Chem. Phys. 17, 807–837. https://doi.org/10.5194/acp-17-807-2017.

Monks, P.S., Archibald, A.T., Colette, A., Cooper, O., Coyle, M., Derwent, R., Fowler, D., Granier, C., Law, K.S., Mills, G.E., Stevenson, D.S., Tarasova, O., Thouret, V., von Schneidemesser, E., Sommariva, R., Wild, O., Williams, M.L., 2015. Tropospheric ozone and its precursors from the urban to the global scale from air quality to short-lived climate forcer. Atmos. Chem. Phys. 15, 8889–8973. https://doi.org/10.5194/acp-15-8889-2015.

Schenkeveld, V.M.E., Jaross, G., Marchenko, S., Haffner, D., Kleipool, Q.L., Rozemeijer, N.C., Veefkind, J.P., Levelt, P.F., 2017. In-flight performance of the ozone monitoring instrument. Atmos. Meas. Tech 10, 1957–1986. https://doi.org/10.5194/amt-10-1957-2017.

Seidel, D., Zhang, Y., Beljaars, A., Golaz, J.-C., Jacobson, A., Medeiros, B., 2012. Climatology of the planetary boundary layer over the continental United States and Europe. J. Geophys. Res. 117 https://doi.org/10.1029/2012JD018143.

Shah, V., Jacob, D.J., Li, K., Silvern, R.F., Zhai, S., Liu, M., Lin, J., Zhang, Q., 2020. Effect of changing NO_x lifetime on the seasonality and long-term trends of satellite-observed tropospheric NO_2 columns over China. Atmos. Chem. Phys. 20, 1483–1495. https://doi.org/10.5194/acp-20-1483-2020.

Sillman, S., 1999. The relation between ozone, NO_x and hydrocarbons in urban and polluted rural environments. Atmos. Environ. 33, 1821–1845. https://doi.org/10.1016/S1352-2310(98)00345-8.

Silvern, R.F., Jacob, D.J., Mickley, L.J., Sulprizio, M.P., Travis, K.R., Marais, E.A., Cohen, R.C., Laughner, J.L., Choi, S., Joiner, J., Lamsal, L.N., 2019. Using satellite observations of tropospheric NO_2 columns to infer long-term trends in US NO_x emissions: the importance of accounting for the free tropospheric NO_2 background. Atmos. Chem. Phys. 19, 8863–8878. https://doi.org/10.5194/acp-19-8863-2019.

Stavrakou, T., Müller, J.-F., Boersma, K.F., De Smedt, I., van der A, R.J., 2008. Assessing the distribution and growth rates of NO_x emission inventories by inverting a 10-year record of NO_2 satellite columns. Geophys. Res. Lett. 35 (10) https://doi.org/10.1029/2008GL033521.

Steinbacher, M., Zellweger, C., Schwarzenbach, B., Bugmann, S., Buchmann, B., Ordonez, C., Prévôt, A.S.H., Hueglin, C., 2007. Nitrogen oxide measurements at rural sites in Switzerland: biasof convential measurement techniques. J. Geophys. Res. 112, D11307. https://doi.org/10.1029/2006JD007971.

Valin, L.C., Russell, A.R., Hudman, R.C., Cohen, R.C., 2011. Effects of model resolution on the interpretation of satellite NO_2 observations. Atmos. Chem. Phys. 11, 11647–11655. https://doi.org/10.5194/acp-11-11647-2011.

van Stratum, B.J.H., Vilà-Guerau de Arellano, J., Ouwersloot, H.G., van den Dries, K., van Laar, T.W., Martinez, M., Lelieveld, J., Diesch, J.-M., Drewnick, F., Fischer, H., Hosaynali Beygi, Z., Harder, H., Regelin, E., Sinha, V., Adame, J.A., Sörgel, M., Sander, R., Bozem, H., Song, W., Williams, J., Yassaa, N., 2012. Case study of the diurnal variability of chemically active species with respect to boundary layer dynamics during DOMINO. Atmos. Chem. Phys. 12, 5329–5341. https://doi.org/10.5194/acp-12-5329-2012.

van der Swaluw, E., Asman, W.A.H., van Jaarsveld, H., Hoogerbrugge, R., 2011. Wet deposition of ammonium, nitrate and sulfate in The Netherlands over the period 1992–2008. Atmos. Environ. 45 (23), 3819–3826. https://doi.org/10.1016/j.atmosenv.2011.04.017.

Veefkind, J.P., de Haan, J.F., Sneep, M., Levelt, P.F., 2016. Improvements to the OMI O_2-O_2 operational cloud algorithm and comparisons with ground-based radar–lidar observations. Atmos. Meas. Tech. 9, 6035–6049. https://doi.org/10.5194/amt-9-6035-2016.

Vestreng, V., Ntziachristos, L., Semb, A., Reis, S., Isaksen, I.S.A., Tarrasón, L., 2009. Evolution of NO_x emissions in Europe with focus on road transport control measures. Atmos. Chem. Phys. 9, 1503–1520. https://doi.org/10.5194/acp-9-1503-2009.

Vilà-Guerau de Arellano, J., van den Dries, K., Pino, D., 2009. On inferring isoprene emission surface flux from atmospheric boundary layer concentration measurements. Atmos. Chem. Phys. 9, 3629–3640. https://doi.org/10.5194/acp-9-3629-2009.

Vilà-Guerau de Arellano, J., van Heerwaarden, C.C., van Stratum, B.J., van den Dries, K., 2015. Atmospheric Boundary Layer: Integrating Chemistry and Land Interactions. Cambridge University Press, New York, USA, p. 265.

Visser, A.J., Boersma, K.F., Ganzeveld, L.N., Krol, M.C., 2019. European NO_x emissions in WRF-Chem derived from OMI: impacts on summertime surface ozone. Atmos. Chem. Phys. 19, 11821–11841. https://doi.org/10.5194/acp-19-11821-2019.

Williams, J.E., Boersma, K.F., Le Sager, P., Verstraeten, W.W., 2017. The high-resolution version of TM5-MP for optimized satellite retrievals: description and validation. Geosci. Model Dev. (GMD) 10, 721–750. https://doi.org/10.5194/gmd-10-721-2017.

Yan, Y., Pozzer, A., Ojha, N., Lin, J., Lelieveld, J., 2018. Analysis of European ozone trends in the period 1995–2014. Atmos. Chem. Phys. 18, 5589–5605. https://doi.org/10.5194/acp-18-5589-2018.

Zara, M., Boersma, K.F., De Smedt, I., Richter, A., Peters, E., van Geffen, J.H.G.M., Beirle, S., Wagner, T., Van Roozendael, M., Marchenko, S., Lamsal, L.N., Eskes, H.J., 2018. Improved slant column density retrieval of nitrogen dioxide and formaldehyde for OMI and GOME-2A from QA4ECV: intercomparison, uncertainty characterization, and trends. Atmos. Meas. Tech. 11, 4033–4058. https://doi.org/10.5194/amt-11-4033-2018.